Half-life of the first excited state of ^{201}Hg

V. Méot,[1,*] J. Aupiais,[2] P. Morel,[1] G. Gosselin,[1] F. Gobet,[3] J. N. Scheurer,[3] and M. Tarisien[3]
[1]*CEA/DIF/DPTA Service de Physique Nucléaire, BP 12, F-91680 Bruyères-le-Châtel, France*
[2]*CEA/DIF/DASE Service de Radioanalyse, Chimie et Environnement, BP 12, F-91680 Bruyères-le-Châtel, France*
[3]*Université Bordeaux 1, CNRS/IN2P3 Centre d'Etudes Nucléaires de Bordeaux Gradignan, UMR 5797 Chemin du Solarium, BP120, F-33175 Gradignan cedex, France*
(Received 30 January 2007; published 12 June 2007)

The lifetime of the first excited state of ^{201}Hg, populated by the ^{201}Tl electron capture decay and subsequent γ-ray transitions, has been measured for the first time. This measurement has been carried out using a coincidence between an internal conversion electron and a γ-ray. The half-life of 81±5 ns has been obtained and $B(E2)$ and $B(M1)$ values were deduced and compared to previous estimates. With these reduced matrix elements, the excitation rate of the first excited state of ^{201}Hg in plasma have been calculated in the frame of a Nuclear excitation by electronic transition (NEET) process.

DOI: 10.1103/PhysRevC.75.064306 PACS number(s): 21.10.Tg, 23.20.Nx, 29.25.Rm, 27.80.+w

The excitation of a nuclear level in plasma has raised significant interest in the scientific community [1–5] with the advent of high intensity laser sources. A method to characterize the phenomenon requires a stable isotope with an isomeric nuclear state at a very low excitation energy, close to the plasma temperature. Some unsuccessful or ambiguous experiments have already been attempted to observe the excitation of the first excited state of ^{235}U and ^{181}Ta in plasma [6–10]. Several authors [11–13] proposed to excite, in a laser heated plasma, the first excited state of ^{201}Hg lying at 1564.8±1.0 eV. The existence of this level was first established by Dragoun *et al.* [14] through the observation of the conversion electron spectrum following its decay. Later, Gerasimov *et al.* [15,16] confirmed this result by observing the lines associated with the outer O subshells. They obtained a value of $\delta^2 = (2.10 \pm 0.55)10^{-4}$ for the multipole $E2/M1$ mixing ratio. Hahn *et al.* [17] have carried out the measurement of the $B(E2)$ using muonic x-ray transitions. They reported two values, $B(E2\uparrow; 3/2^- \rightarrow 1/2^-) = 0.104 \pm 0.024\, e^2\,\mathrm{b}^2$ and $B(E2\uparrow; 3/2^- \rightarrow 1/2^-) = 0.145 \pm 0.022\, e^2\,\mathrm{b}^2$ determined from a M-transition or K and L-transition x-rays, respectively. However due to the lack of information on the nuclear spectroscopy of ^{201}Hg, their analysis was hampered and no conclusion was drawn. Using the weighted average of both values, $B(E2\uparrow; 3/2^- \rightarrow 1/2^-) = 0.127 \pm 0.017\, e^2\,\mathrm{b}^2$, the half-life of the level has been approximately estimated at 60 ns [18]. The design of a plasma experiment requires the precise knowledge of the lifetime for both calculation of the excitation rate and experimental signature of the process. Here, we report the first measurement of the half-life of the 1.565 keV level. The measured half-life and a calculated internal conversion coefficient will enable us to extract the reduced transition rates. Using those with the model described in [5], we calculated the nuclear excitation by electronic transition (NEET) rate of the 1.565 keV level in plasma at local thermodynamic equilibrium (LTE).

In the present experiment, the 1.565 keV ^{201}Hg level is populated by the electron-capture decay of ^{201}Tl (72.912-h half-life). The ^{201}Hg levels reached by this decay are shown in Fig. 1 [18,19]. The 1.565 keV level is fed either directly (43% per ^{201}Tl decay) or from the 167.4 keV and 32.2 keV level decays, filled in 43.6% and 13.3% per ^{201}Tl decay, respectively. The measurement consists of performing a delayed coincidence between an electron coming from the internal conversion of the 1.565 keV level and a γ-ray emitted from a transition feeding this level.

The ^{201}Tl source is supplied as thallium chloride in isotonic solution by CIS Bio International (Gif-sur-Yvette, France) with an initial activity of 140 MBq. The production of the source is performed by the reaction ^{203}Tl $(p, 3n)^{201}$Pb followed by the ^{201}Pb decays (9.4 h half-life) to ^{201}Tl.

The kinetic energies of the 1.565 keV conversion electrons are gathered in Table I [20]. Their inelastic mean free paths in matter are shorter than 10 Å which implies making a very thin source. For that purpose, a platinum disk (Ø = 20 mm, 25 μm thick) is prepared for electroplating by cleaning it successively with acetone, alcohol and water. The 1 ml isotonic solution of ^{201}Tl is diluted in a 20 ml 5M NH_4Cl solution. Then the solution is electroplated on the platinum disk by fixing the current at about 0.5 A for 30 minutes. Just before the end, a few drops of concentrated ammoniac solution are added to the cell to prevent a possible dissolution of the electroplated mercury and thallium. The cell is emptied and voltage is switched off after all the solution has been removed. The platinum disk is finally washed in water and alcohol, successively. The electroplating technique gives a uniform layer thickness. As the weight of the deposit is less than 20 ng, the thickness may be estimated to a few Ångström. The amount of ^{201}Tl on substrate was determined from its activity, 10 MBq just after the electrodeposition, measured by γ spectroscopy. Figure 2 shows the γ-ray spectrum of the ^{201}Tl deposit obtained with a high purity germanium detector. The decay of ^{201}Tl to ^{201}Hg is identified by the 135.3 keV and 167.4 keV ^{201}Hg γ-ray lines. The 439 keV γ-ray line originates from the ^{202}Tl decay contaminant (12.23 d half-life). At lower energy, the background 238.5 keV γ-ray line disappears under

*vincent.meot@cea.fr; URL: http://www-phynu.cea.fr/

TABLE I. Conversion electron energies following the decay of 1.565 keV level obtained from [20].

Atomic shell	$4s_{1/2}$ $(N1)$	$4p_{1/2}$ $(N2)$	$4p_{3/2}$ $(N3)$	$5s_{1/2}$ $(O1)$	$5p_{1/2}$ $(O2)$	$5p_{3/2}$ $(O3)$
Kinetic energy (eV)	762	884	988	1445	1481	1500

coincidence conditions. Below 80 keV, the mercury x-rays are seen.

The electrons were detected with a channel electron multiplier (channeltron X951BL PHOTONIS) operating in saturated mode. The ^{201}Tl source was positioned inside a stainless steel vacuum chamber 10 mm in front of the channeltron. A dry primary vacuum pump associated with a cryogenic pump allowed operating in a 10^{-7} mbar vacuum while preventing oil deposition on the sample. The deposit sample was biased by a positive voltage while the head of the channeltron is kept at ground potential. By varying this voltage, we were able to select electrons with a kinetic energy greater than the electric potential and, thus to suppress the numerous low energy electrons (Auger, backscattered electrons,. . .)

For the lifetime measurement, the γ-rays were detected by a $1i \times 1i$ $LaBr_3$:Ce crystal scintillator (BrilLanCe® 380)

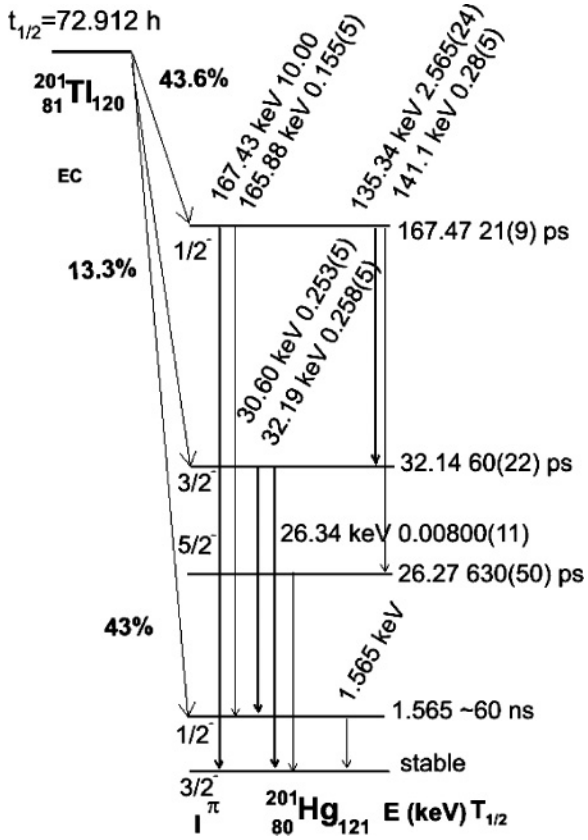

FIG. 1. Detailed decay scheme of ^{201}Tl [18,19]. The γ-ray intensities, listed after the γ-ray energies, are specified per 100 decays of ^{201}Tl.

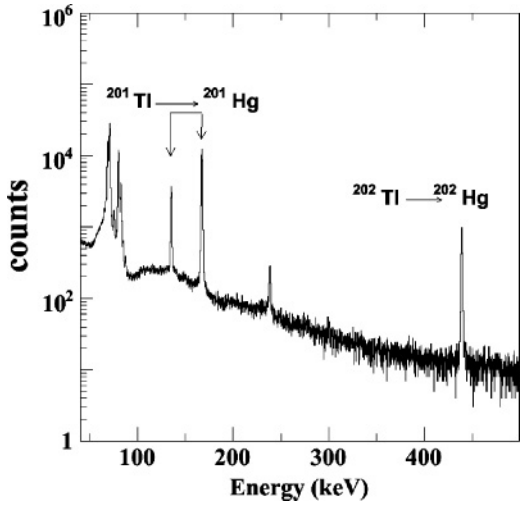

FIG. 2. A γ-ray spectrum of the ^{201}Tl deposit obtained with a high purity germanium detector.

coupled to a XP2060B phototube. The fast decay time and the energy resolution of the $LaBr_3$:Ce crystal are very attractive for this application. The crystal was positioned outside the vacuum chamber at 1cm from the source. At this position the aluminium window chamber is 1 mm thick. The crystal was protected from the intense x-ray emission by a 0.4 mm sheet of cadmium. The detection efficiency was determined using a ^{152}Eu source set at the source position. Figure 3 shows the γ-ray spectrum in coincidence with electrons for a +600 V applied potential.

The measurement consists of performing an event by event γ-e^- correlation using a 600 ns coincidence window. A time-to-amplitude converter (TAC) was started by a signal from a coincidence between both detectors, and stopped by the delayed signal from the scintillation detector. The TAC spectrum is shown Fig. 4. The prompt peak is produced by

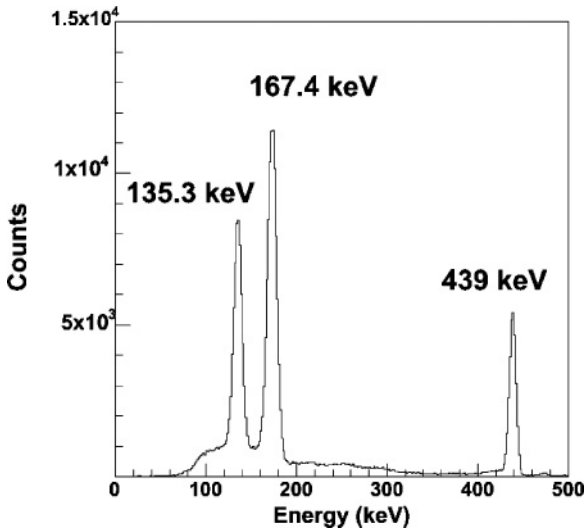

FIG. 3. A γ-ray spectrum of the ^{201}Tl deposit obtained with a $LaBr_3$:Ce crystal in coincidence with the channeltron detector.

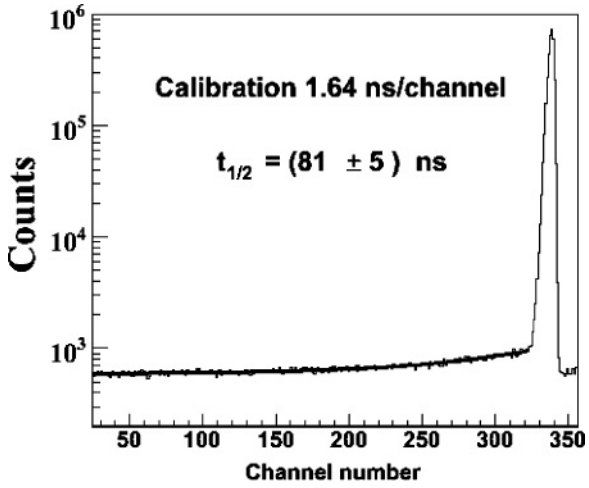

FIG. 4. TAC spectrum for γ-rays in coincidence with electrons. The applied voltage on the source deposit is +600 V.

the huge number of conversion and Auger electrons emitted by the source in coincidence with γ-rays. The asymmetry of the prompt peak is due, for a large part, to the differing times of flight of the various Auger electrons. For kinetic energies associated to the 1.565 keV internal conversion electrons (Table I) we calculated the time of flight distribution for a +600 V applied potential. The slightly asymmetric distribution is centred on 1 ns with a root mean square of 0.3 ns. Hence, concerning the 1.565 keV conversion electrons, the influence of the time of flight on the TAC spectrum is negligible.

The delayed component observed Fig. 4 was fitted by an exponential function plus a constant background. The half-life was extracted to be $t_{1/2} = (81 \pm 5)$ ns for the best reduced χ^2 value of 1.021.

Figure 5 shows the TAC spectra gated by γ-rays of 135.3 keV, 167.4 keV, and 439 keV energies for a +600 V applied potential. A delayed component is clearly measured for electrons in coincidence with the 135.3 keV and 167.4 keV γ-ray lines whereas the background intensity has a flat time distribution for the 439 keV γ-ray energy coming from the decay of ^{202}Tl. The observed half-lives are (82.0±2.1) ns for a reduced χ^2 value of 1.11 and (72±13) ns for a reduced χ^2 value of 0.81, for the 135.3 keV and 167.4 keV, respectively. The amplitude of the delayed signal is (10.3±3.8) times smaller for the 167.4 keV γ-ray than for the 135.3 keV one. The first one comes from the unresolved 165.9 keV γ-ray. The 1.565 keV level is fed by the 135.3 keV radiative transition followed by the 30.6 keV transition at a 52% relative intensity when the internal conversion process is involved. Taking into account the 1.565 keV state feeding intensities by the 165.9 keV and 135.3 keV, respectively, 0.00155 and 0.0134 per ^{201}Tl decay, and the detection efficiency, the expected ratio is 9.2 compatible with our experimental ratio.

In order to check that the delayed signal comes from the level located at 1.565 keV, the bias on the source was varied up to +1600 V beyond which no delayed signal was expected. As shown on Fig. 6, the intensity of the delayed component decreases with increasing voltages and disappears beyond

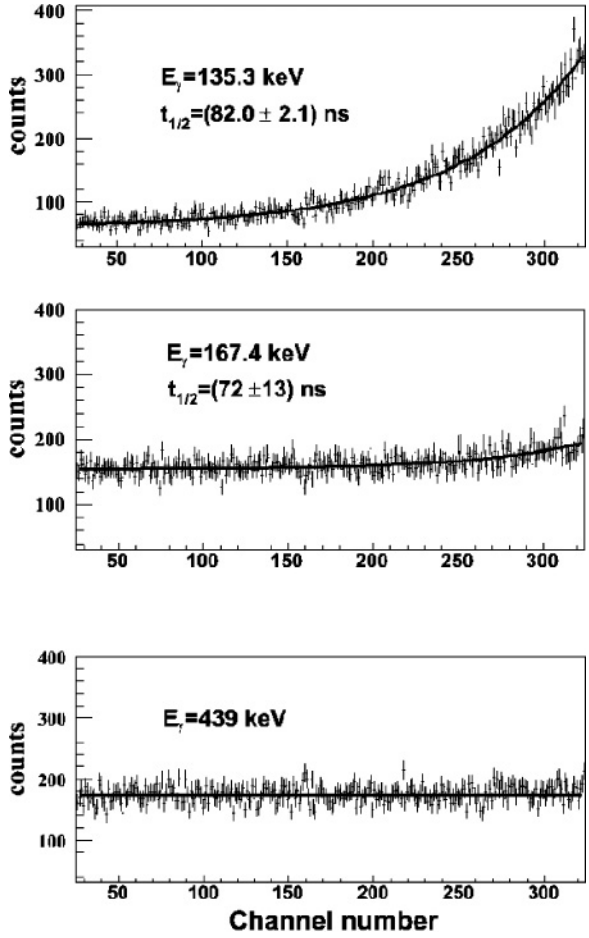

FIG. 5. TAC spectra gated on the 135.3 keV, 167.4 keV, and 439 keV γ-rays energies. The applied voltage on the source deposit is +600 V.

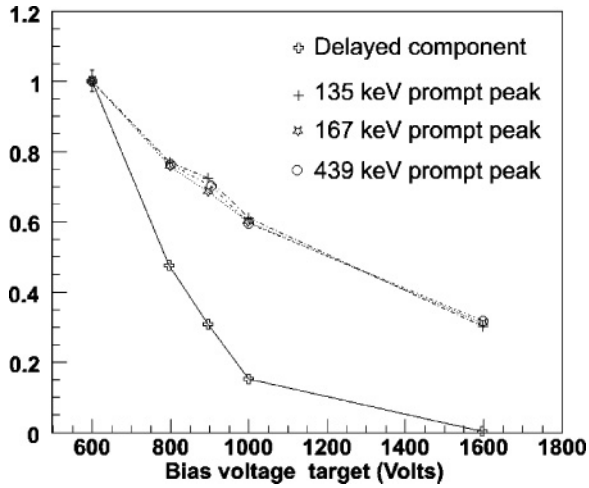

FIG. 6. Normalized intensity of the delayed component and prompt peak gated on the 135 keV, 167 keV, and 439 keV γ-rays energies versus the bias voltage target (the solid curves serve only to guide the eyes).

TABLE II. Relative intensities of conversion electrons following the 1.565 keV level decay. Experimental and theoretical intensities are obtained from [14,15] and [21], respectively.

Mixing ratio Subshells ratio	$\delta^2 = (2.10 \pm 0.55)10^{-4}$ [15]		$\delta^2 = (1.1 \pm 0.3)10^{-4}$ [14]	
	Experimental	Theoretical	Experimental	Theoretical
$N1/N2$	0.94±0.31	0.74	1.19±0.30	1.32
$N2/N3$	0.64±0.05	0.76	0.92±0.15	0.82
$N1/N3$	0.6±0.2	0.57	1.1±0.2	1.08
$O1/N2$	0.128±0.030	0.14		0.29
$O2/N3$	0.158±0.030	0.13		0.16
$O3/N3$	0.20±0.04	0.17		0.18

+1600 V. We plotted on the same graph the variations of the prompt peak intensity in the TAC spectrum gated on each of the three γ peaks. For each set, the data were normalized at their +600 V value. The variations with the bias voltage are very similar but differ from that of the delayed component, which means the underlying electron spectrum is different. This difference mainly comes from the high energy Auger electrons.

From these various results, the lifetime of the 1.565 keV level is assigned without ambiguity to (81±5) ns which corresponds to the best reduced χ^2 value.

In order to extract the reduced matrix elements $B(E2; 1/2^- \rightarrow 3/2^-)$ and $B(M1; 1/2^- \rightarrow 3/2^-)$, the internal conversion coefficients calculated by Band and Trzhaskovskaya [21] for the 1.565 keV ^{201}Hg transition were used. In this approach the bound and free electron wave functions are obtained in the relativistic Dirac-Fock atomic field. The calculations are based on the nuclear model of a uniform charge distribution over the volume of a spherical nucleus. The surface currents of the transition inside the nucleus and holes in the shell from which the electron is converted are taken into account. Table II displays the relative intensities of the partial conversion coefficients compared to the experimental ones [14–16]. Using both the mixing ratio values of $(2.10 \pm 0.55)10^{-4}$ [15] and $(1.1 \pm 0.3)10^{-4}$ [14], we obtain a total conversion coefficient of $(6.50 \pm 1.25)10^4$ and $(4.23 \pm 0.68)10^4$, respectively.

From the calculated internal conversion coefficient, the $E2/M1$ multipole mixing ratio and the measured lifetime, we can derive the reduced matrix elements. Table III shows the extracted $B(E2)$ and $B(M1)$ using both mixing ratios. The $B(E2; 1/2^- \rightarrow 3/2^-)$ obtained with the mixing ratio value from [15] is very close to weighted average $B(E2; 1/2^- \rightarrow 3/2^-) = 0.254 \pm 0.034\, e^2\,\mathrm{b}^2$ value obtained from muonic x-ray transitions [17] corrected by the spin ratio $(2j_i+1)/(2j_f+1) = 2$, where j_i and j_f are the initial and final total angular momentum, respectively. Although both extracted $B(E2)$ values are compatible, in the following we will use the reduced matrix elements obtained with the mixing ratio of $(2.10 \pm 0.55)10^{-4}$. Contrary to [14], the mixing ratio in [15] is obtained with the lines associated with the outer O subshells whose uncertainties are the lowest. As discussed in [15], the disagreement could arise from a different treatment of Auger and backscattering electrons.

With these reduced matrix elements, we calculated the NEET [22–24] rate of the 1.565 keV in plasma. The NEET process is a resonant process involving both the excitation of the nucleus and the deexcitation of the atomic system by an electronic transition between two atomic bound states. Some difficulties arise in observing this effect. On the one hand, the coupling matrix element between atomic and nuclear systems is very low because it strongly depends on the presence of the electrons close to the nucleus. On the other hand, the matching between the nuclear and electronic transitions may be poor. Because both quantities depend on the electronic configuration, the NEET probability can be enhanced by modifying the atomic environment of the nucleus. In hot dense plasmas, the thermodynamic conditions strongly affect the electronic environment of the ions. Thus, plasmas are ideal laboratories to observe these modifications of nuclear rates. However, a calculation of the NEET process in plasma needs to have a precise description of the atomic properties and an accurate representation of the statistical nature of the electronic spectrum. A NEET model in plasma at LTE has recently been worked out [5]. The most relevant hydrodynamic parameters, such as charge state, density or temperature were calculated

TABLE III. Extracted $B(E2)$ and $B(M1)$ as a function of the mixing ratio and internal conversion coefficient.

Mixing ratio	Internal conversion coefficient	$B(E2; 1/2^- \rightarrow 3/2^-)$	$B(M1; 1/2^- \rightarrow 3/2^-)$
$(2.10 \pm 0.55)10^{-4}$	$(6.50 \pm 1.25)10^4$	$0.249 \pm 0.082\, e^2\,\mathrm{b}^2$	$(2.0 \pm 0.7)10^{-3}\mu_N^2$
$(1.1 \pm 0.3)10^{-4}$	$(4.23 \pm 0.68)10^4$	$0.194 \pm 0.062\, e^2\,\mathrm{b}^2$	$(3.0 \pm 0.5)10^{-3}\mu_N^2$

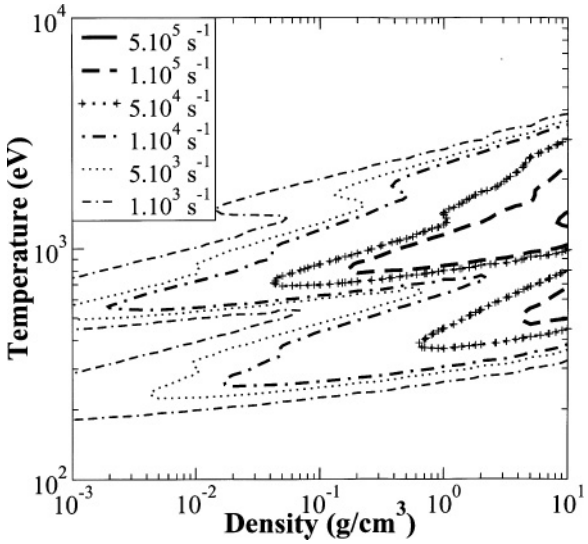

FIG. 7. NEET rate map of the 1.565 keV level as a function of the plasma density and temperature.

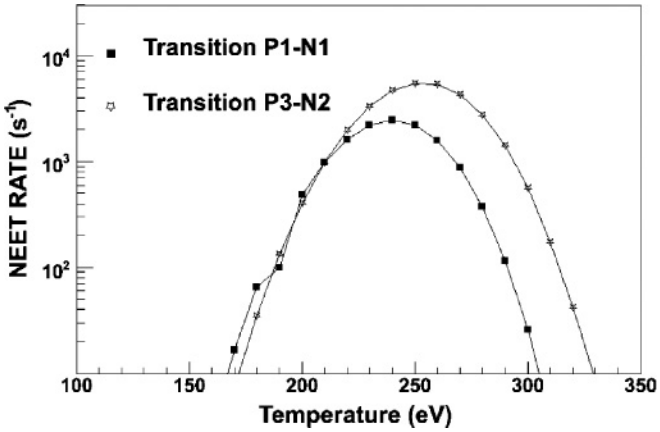

FIG. 8. NEET rate of the 1.565 keV level of ^{201}Hg as a function of the plasma temperature. Although creating LTE plasma at 250 eV is a difficult task, this calculation may be useful to design an experiment.

under the LTE hypothesis using a relativistic average atom model [25]. Our NEET model takes into account the statistical nature of the electronic spectrum using a Gaussian distribution of the configurations [26] around the transition given by the average relativistic atom model. It enables to derive a transition rate as a function of the temperature T and the density ρ of the plasma. We applied this calculation to the excitation of the first isomeric state of ^{201}Hg for a broad range of temperatures and densities.

According to Ref. [5], we express the NEET rate as

$$\lambda^{\mathrm{NEET}}(\rho, T) = \frac{2\pi}{\hbar} D_i p_i (1 - p_f) |R_{i,f}|^2 \frac{1}{\sqrt{2\pi\sigma^2}} e^{-\frac{\delta^2}{2\sigma^2}},$$

where the subscripts i and f label the initial and final orbital, respectively, p is the occupation probability of an orbital with degeneracy D, given by the Fermi-Dirac statistics, δ is the mismatch energy between the atomic and the nuclear transition and σ the energy variance describing the dispersion of the electronic transition energy of real configurations around the average atom value. $|R_{i,f}|^2$ is the coupled atom-nucleus matrix element defined in [5].

Figure 7 shows the map of the NEET rate of the excitation of the first isomeric state of ^{201}Hg. It strongly depends on thermodynamic conditions. Variations of the temperature or density modify the atomic transition energy and thus the mismatch. Another feature apparent in Fig. 7 is that the rate originates from a small number of electronic transitions. Two areas are favorable to the NEET mechanism. They are found around a temperature of 250 and 630 eV assuming a plasma density of 10^{-2} g/cm^3 (cutoff density for 0.53 μm laser wavelength). The first zone corresponds to $6s_{1/2}$-$4s_{1/2}$ ($P1$-$N1$) and $6p_{3/2}$-$4p_{1/2}$ ($P3$-$N2$) electronic transitions, the second one to $5p_{3/2}$-$4p_{1/2}$ ($O3$-$N2$) and $5s_{1/2}$-$4p_{1/2}$ ($O1$-$N1$) electronic transitions. The average ionic charges under both thermodynamic conditions, 250 eV and 630 eV, for 10^{-2} g/cm^3, are around 44^+ and 61^+, respectively. The latter ionic charge is too high to be reached in a laser experiment, so we will focus on the former.

Figure 8 shows the NEET rate for both $P3$-$N2$ and $P1$-$N1$ resonant transitions at 10^{-2} g/cm^3. The coupled atom-nucleus matrix elements are 2.9 10^{-8} eV^2 and 2.7 10^{-8} eV^2 for the $P3$-$N2$ and $P1$-$N1$ transition, respectively. Compared to the ^{235}U case [5], the higher strength of the ^{201}Hg NEET rate (a few 10^3s^{-1}) is mainly due to the nuclear part of the matrix element.

In summary, we have measured the half-life of the first excited state of ^{201}Hg, located at 1.565 keV, to be (81±5) ns. With this value and using reliable theoretical conversion coefficients, the $E2$ and $M1$ transition rates were extracted. Our $B(E2)$ transition rate is in a good agreement with the value obtained from muonic x-ray transitions. Using these reduced nuclear matrix elements, we calculated the NEET rate of the 1.565 keV level in LTE plasma. The NEET rate peaks at few 10^{+5} s^{-1} for the higher plasma density whereas in ^{235}U it only reaches a few 10^{-4} s^{-1}. The precise knowledge of the lifetime and the NEET rate will enable us to explore the excitation of this nuclear state in plasma.

[1] K. W. D. Ledingham, P. McKenna, and R. P. Singhal, Science **300**, 1107 (2003).
[2] T. J. Burvenich, J. E. Christoph, and H. Keitel, Phys. Rev. C **74**, 044601 (2006).
[3] G. A. Mourou, T. Tajima, and S. V. Bulanov, Rev. Mod. Phys. **78**, 309 (2006).
[4] G. Gosselin and P. Morel, Phys. Rev. C **70**, 064603 (2004).
[5] P. Morel, V. Méot, G. Gosselin, D. Gogny, and W. Younes, Phys. Rev. A **69**, 063414 (2004).
[6] Y. Izawa and C. Yamanaka, Phys. Lett. **B88**, 59 (1979).
[7] R. V. Arutyunyan *et al.*, Sov. J. Nucl. Phys. **53**, 23 (1991).
[8] G. Claverie *et al.*, Phys. Rev. C **70**, 044303 (2004).
[9] F. Gobet *et al.*, Rev. Sci. Instrum. **77**, 093302 (2006).

[10] A. V. Andreev, R. V. Volkov, and V. M. Gordienko, JETP **91**, 1163 (2000).
[11] M. R. Harston and J. F. Chemin, Phys. Rev. C **59**, 2462 (1999).
[12] A. V. Andreev, V. M. Gordienko, A. B. Savel'ev, E. V. Tkalya, and A. M. Dykhne, JETP Lett. **66**, 331 (1997).
[13] E. V. Tkalya, Laser Phys. **14**, 360 (2004).
[14] O. Dragoun, V. Brabec, M. Ryšavý, A. Špalek, and K. Freitag, Z. Phys. A **326**, 279 (1987).
[15] V. N. Gerasimov, D. V. Grebennikov, V. M. Kulakov, S. K. Lisin, and V. V. Kharitonov, Phys. At. Nucl. **60**, 1780 (1997).
[16] V. V. Kharitonov and V. N. Gerasimov, Phys. At. Nucl. **65**, 1377 (2002).
[17] A. A. Hahn, J. P. Miller, R. J. Powers, A. Zehnder, A. M. Rushton, R. E. Welsh, A. R. Kunselman, and P. Roberson, Nucl. Phys. **A314**, 361 (1979).
[18] F. G. Kondev, ENSDF (2005), URL: http://www.nndc.bnl.gov/.
[19] B. M. Coursey, D. D. Hoppes, A. T. Hirschfeld, S. M. Judge, D. H. Woods, M. J. Woods, E. Funck, H. Schrader, and A. G. Tuck, Appl. Radiat. Isot. **41**, 289 (1990).
[20] R. B. Firestone, V. S. Shirley, C. M. Baglin, S. Y. F. Chu, and J. Zipkin, *Table of Isotopes* (John Wiley and Sons, New York, 1996, 1998, 1999).
[21] I. Band and M. B. Trzhaskovskaya, Bull. Acad. Sci. USSR, Phys. Ser. **55**, 59 (1991).
[22] M. Morita, Progr. Theor. Phys. **49**, 1574 (1973).
[23] E. V. Tkalya, Nucl. Phys. **A539**, 209 (1992).
[24] M. Harston, Nucl. Phys. **A690**, 447 (2001).
[25] B. F. Rozsnyai, Phys. Rev. A **5**, 1137 (1972).
[26] G. Faussurier, C. Blancard, and A. Decoster, Phys. Rev. E **56**, 3488 (1997).